ACS OMEGA

http://pubs.acs.org/journal/acsodf

Article

Investigation on Electroreduction of CO_2 to Formic Acid Using $Cu_3(BTC)_2$ Metal–Organic Framework (Cu-MOF) and Graphene Oxide

Sun-Mi Hwang, Song Yi Choi, Min Hye Youn, Wonhee Lee, Ki Tae Park, Kannan Gothandapani, Andrews Nirmala Grace,* and Soon Kwan Jeong*

Cite This: *ACS Omega* 2020, 5, 23919–23930

Read Online

ACCESS | Metrics & More | Article Recommendations | Supporting Information

ABSTRACT: A recent class of porous materials, viz., metal–organic frameworks (MOFs), finds applications in several areas. In this work, Cu-based MOFs (Cu–benzene-1,3,5-tricarboxylic acid) along with graphene oxide, viz., Cu-MOF/GO, are synthesized and used further for reducing CO_2 electrochemically. The reduction was accomplished in various supporting electrolytes, viz., $KHCO_3/H_2O$, tetrabutylammonium bromide (TBAB)/dimethylformamide (DMF), KBr/CH_3OH, CH_3COOK/CH_3OH, TBAB/CH_3OH, and tetrabutylammonium perchlorate (TBAP)/CH_3OH to know their effect on product formation. The electrode fabricated with the synthesized material was used for testing the electroreduction of CO_2 at various polarization potentials. The electrochemical reduction of CO_2 is carried out via the polarization technique within the experimented potential regime vs saturated calomel electrode (SCE). Ion chromatography was employed for the analysis of the produced products in the electrolyte, and the results showed that HCOOH was the main product formed through reduction. The highest concentrations of HCOOH formed for different electrolytes are 0.1404 mM (−0.1 V), 66.57 mM (−0.6 V), 0.2690 mM (−0.5 V), 0.2390 mM (−0.5 V), 0.7784 mM (−0.4 V), and 0.3050 mM (−0.45 V) in various supporting electrolyte systems, viz., $KHCO_3/H_2O$, TBAB/DMF, KBr/CH_3OH, CH_3COOK/CH_3OH, TBAB/CH_3OH, and TBAP/CH_3OH, respectively. The developed catalyst accomplished a significant efficiency in the conversion and reduction of CO_2. A high faradic efficiency of 58% was obtained with 0.1 M TBAB/DMF electrolyte, whereas for Cu-MOF alone, the efficiency was 38%. Thus, the work is carried out using a cost-effective catalyst for the conversion of CO_2 to formic acid than using the commercial electrodes. The synergistic effect of GO sheets at 3 wt % concentration and Cu^+OH^- interaction leads to the formation of formic acid in various electrolytes.

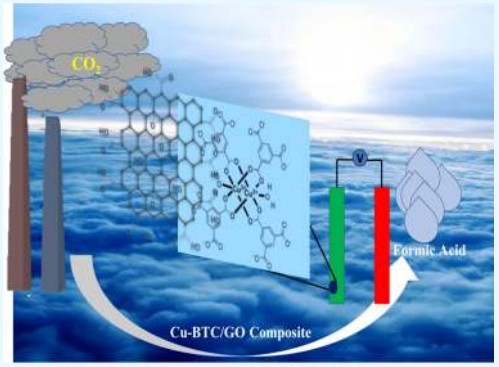

INTRODUCTION

A surfeit of interest has been laid on CO_2 fixation due to global warming and its devastating consequences with an alarming increase in the CO_2 level in the atmosphere.[1,2] Out of the various routes to control CO_2 emissions, CO_2 reduction to valuable compounds or fuels by a photochemical or an electrochemical process has gained huge interest.[3−6] As a liquid fuel, the generated energy on storage can be transported freely or regenerated to electricity by fuel cells.[7] The electrochemical process, if made efficient, could become a viable method for the synthesis of liquid fuels in the time to come.[8,9] Direct electroreduction at noble metal or carbon electrodes requires a substantial overpotential, and hence, a suitable choice of a more active metal as the working electrode can result in lower overpotentials and a variety of reduction products.[10,11] The main issue in the electrochemical reduction process is the requirement of high potential.[12] For instance, the reduction of CO_2 to $CO_2^{\bullet-}$, which is a one-electron step, needs −1.90 V potential vs standard hydrogen electrode (SHE).[12] In the case of the reduction process using many electrons, it needs a less potential, say −0.38 V, for six electrons to get converted to methanol; thus, any reaction proceeding without any catalyst will have to cross through this challenging step. This urges to use new materials as electrocatalysts, which can permit reduction that needs a many-electron process to progress via an inner sphere pathway mechanism.[13] Metal-based electrochemical systems have been investigated expansively, and it has been established that the reduction products depend sturdily on the electrode materials.[14] Azuma et al. grouped the products obtained from various metal electrodes for the CO_2 reduction process.[15] For an effective reduction, the role of the catalyst should promote the charge-

Received: July 1, 2020
Accepted: September 3, 2020
Published: September 14, 2020

https://dx.doi.org/10.1021/acsomega.0c03170
ACS Omega 2020, 5, 23919–23930

Scheme 1. Schematic of the Synthesis of the Cu-MOF/GO Composite

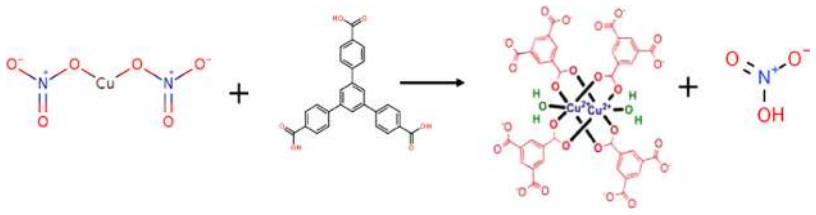

transfer process across the electrode, a less overpotential in a hydrophilic atmosphere to give converted products.[16] An efficient reduction process is rated in terms of the faradic efficiency, formation of selective products, which in turn depends on the fabricated electrode, concentration of the analyte, nature of the electrolyte, redox potential, etc.[17−26] In the electrochemical CO_2 conversion process, the imperative factor deciding the efficiency are electrode materials and electrolyte systems.[27,28] Such properties are exhibited by metals like Cd, Pb, Ag, In, Cu, etc., and these metal possess a large overpotential for H_2 production and are regarded as good catalysts, facilitating the reduction process.[29] In spite of these efforts, the process lacks efficiency, and in this regard, it is imperative to find alternative and efficient catalysts that can deliver the product with good efficiency and at a reduced overpotential. Several catalysts are investigated for the reduction process like Sn, Pb, and Ru for reducing and converting CO_2 to fuels.[30−32] Other types of materials including polymers, metal−organic frameworks (MOFs), and polymer composites have been reported.[32,33] In recent times, Cu-based compounds are documented for their excellent activity,[34,35] and the copper ions help in the reduction process. Most of the metal catalysts show a limited catalytic activity as H_2 gas is evolved during the reduction process due to water electrolysis and is regarded as the impeding step. Reports suggest that the reduction process in general yields CO, CH_3OH, or HCOOH. In the case of the latter, the reduction involves a potential as high as −1.5 V with reference to the standard hydrogen electrode.[36] Copper is investigated for converting CO_2 to hydrocarbons and is the most investigated catalyst, but the process involving Cu gives many reaction products, thus lacking selectivity, and to cater the same, alloys have been reported for the reduction.[37]

In such cases, the reaction sites with protons get altered through the modification of the adjacent reaction sites, facilitating the reduction of CO_2. The attention toward metal-organic frameworks (MOFs) has amplified exponentially due to their interesting structural properties and imperative potential applications.[38] These materials are a category of innovative porous structures with a periodicity and are governed by the covalent bonding system and also through attractive forces between the molecules containing organic linkers attached to metal ions.[39] Particularly, MOFs have acknowledged more consideration in electrochemical applications. The electrocatalytic reduction of CO_2 has been verified with Cu-MOF films.[40] As equated to MOF materials, heterogeneous nanostructured materials with carbon composites have been investigated for sensing applications.[41] Such composites with frameworks not only act as catalysts but also provide good conductivity and stability.[42−45] The exclusive electronic nature of the two-dimensional (2D) material, viz., graphene, aids in the reduction process and improves the reaction kinetics. Various reports exist on the investigation of graphene-based materials aimed at electrochemical besides photochemical CO_2 reduction,[46−50] wherein it is clear that graphene has contributed substantially in the reduction process. In the earlier work on Cu_2O nanocomposites, formic acid was the main product.[51] Many MOFs and composites have been used for various applications like hydrogen evolution reaction (HER), oxygen evolution reaction (OER), and methanol oxidation reaction.[52−55] In yet another report, Cu_2O and ZnO composites in various ratios were employed for the electrochemical reduction of CO_2 to obtain 17.7 and 16.8% faradaic efficiency to produce methanol.[56−58] Various Cu-based MOF were used as catalysts for CO_2 reduction to produce methanol with faradaic efficiency of 15.9, 1.2, 6, and 9.9%, respectively.[59] Further, in yet another report, a Cu- and Bi-based bimetallic metal−organic framework was used as a catalyst in the $KHCO_3$ electrolyte, which gave methanol at a selective efficiency of 18.2%.[60] Zirconium-based MOFs were prepared and electrochemical CO_2 reduction was carried out in the aqueous electrolyte, leading to the formation of formic acid.[61] With all of these developments, this work is aimed at making a composite of Cu-based MOF with graphene oxide sheets and further investigating its applicability in the electroreduction of CO_2.[62−66]

EXPERIMENTAL SECTION

Materials. Copper nitrate (99.99%), benzene tricarboxylic acid (BTC, 95%), dimethylformamide (DMF), tetrabutylammonium perchlorate (TBAP), copper sulfate, and methanol were received from SIGMA and used for the synthesis without any further purification. All other solvents were procured from local suppliers and used without further purification. Carbon papers were purchased from Ballard.

Synthesis of Cu-MOF/GO by a Hydrothermal Route. Cu-MOF/GO was synthesized in accordance with the previous report but through a slight amendment in the presence of GO.[52] $Cu(NO_3)_2$ (1.75 g, 7.2 mmol) was stirred with the required amount of benzene-1,3,5-tricarboxylic acid (0.84 g, 4 mmol) for 20 min in a mixture of solvents, viz., DMF/EtOH/H_2O (1:1:1), in a slurry form. GO (80 mg, 3 wt %) was added to it. The final mixture was agitated for an additional 30 min, transferred to an autoclave, and subjected to a heat treatment of 100 °C for 24 h. The obtained product was then stored in a desiccator for further use. A schematic of the synthesis procedure is given in Scheme 1.

In the Cu-BTC water solvent system, copper nitrite is used as a copper source and benzene-1,3,5-tricarboxylic acid as a proton source (ligand). Cu-BTC complexation of Cu^{2+} takes place with the formation of the water molecule complex, viz., $[Cu(H_2O)_3(OH)]^{2+}$, wherein a Cu^{2+} cation strongly complexes with a water molecule reduced from a hydroxide source.

$$2Cu(NO_3)_2 + 2H_3BTC \rightarrow Cu_3(BTC)_2 \cdot 3H_2O + 6HNO_3 \quad (1)$$

https://dx.doi.org/10.1021/acsomega.0c03170
ACS Omega 2020, 5, 23919−23930

From eq 1, all absorbed protons slowly increase the pH level as desired for the formation of $[Cu_3(BTC)_2]$ units, hydroxide anions, and oxides along with the deprotonation of H_3BTC.

Instrumentation. X-ray diffraction (XRD) was done using a Rigaku Miniflex instrument with a Cu Kα (1.5406 Å) radiation. The X-ray photoelectron spectroscopy (XPS) measurement was done with a Thermo Scientific instrument, and the same was corrected for carbon by 284.6 eV. The surface morphologies of the thin film were investigated using a Hitachi model field-emission scanning electron microscope (FE-SEM). The products dissolved in the electrolyte, viz., HCOOH and acetic acid, were analyzed using ion chromatography (Metrohm 881) in 1 mM $HClO_4$ with acetone (5%) and 10 mM LiCl as the suppressor. In our work, only the liquid was analyzed with the importance given to understand the formation of formic acid, and all of the dilution factors were taken for analyses and calculations. Further, the liquid products were investigated using the high-performance liquid chromatography (HPLC; Agilent HPLC-1200 series) technique with a UV detector, with the column being Aminex HPX-87H, 300 mm × 7.8 mm, and the mobile phase used for the study being 5 mM H_2SO_4.

Electrochemical Investigation. The reduction test was conducted at a Biologic SP-240 test station using a three-probe system, and all of the measurements were performed using a saturated calomel electrode as a reference. The working electrode where reduction takes place was carbon paper, and the loop was closed using Pt as a counter electrode. The catalyst was drop-casted on carbon paper, dried, and further employed as the working probe for the CO_2 reduction process. During the process, the constant current potential technique was adopted by applying a range of potentials for different electrolytes.

CO_2 Electroreduction Test. CO_2 electroreduction was performed in an H-type cell separated by a proton exchange membrane in various electrolytes (Scheme 2). The catholyte was saturated with pure CO_2, and the electrolyte was continuously stirred by a magnetic bar during electrolysis. CO_2 electroreduction was performed in six different electrolyte systems, viz., $KHCO_3/H_2O$, TBAB/DMF, KBr/CH_3OH, CH_3COOK/CH_3OH, $TBAB/CH_3OH$, and $TBAP/CH_3OH$, to know their effect on the product formation, wherein TBAB is tetrabutylammonium bromide and TBAP is tetrabutylammonium perchlorate. All of the supporting electrolytes taken for the study have a 0.1 M concentration. Initially, to saturate the system, 100 sccm pure CO_2 was purged into the electrolyte for a duration of 1 h. During the process, the system is kept under continuous stirring.

Scheme 2. Schematic of the H-Type Membrane Based Electrochemical Cell

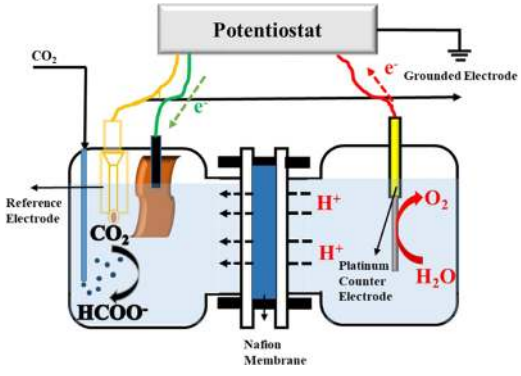

The as-fabricated MOF electrodes were placed at the cathode part, and the saturated calomel electrode (SCE) (sat. KCl) and platinized Pt wire was kept at the anode part. For the electroreduction, techniques like cyclic voltammetry and constant-potential technique were used to find the current density and faradic efficiency, respectively. The cathodic potential was measured with respect to SCE that was connected with the catholyte through the membrane. Initially, 100 sccm CO_2 gas was bubbled into the catholyte for 1 h. For determining the current density and faradic efficiency, cyclic voltammogram (CV) tests were performed and chronopotentiometry tools were used. The electrochemical reduction was carried out by the polarization technique operated within the potential range, and this range was fixed after a lot of iterations for each supporting electrolyte system. Ion chromatography was further used to analyze the products obtained after the reduction process dissolved in the electrolyte with an interest in HCOOH. Each experiment was performed twice, and the mean value was stated. To calculate the faradic efficiencies, the following formula is used

$$F{\cdot}E[\eta]\ (\%) = \frac{mnF}{\int_0^t I\,dt}$$

where m represents the number of moles of product formed, n is the number of electrons required, F is the Faraday constant (96 485 C/mol of electrons), and I is the current.

RESULTS AND DISCUSSION

X-ray diffraction results of the Cu-MOF/GO material prepared by the hydrothermal technique are shown in Figure 1. The spectrum shows pristine H-KUST-1 with the FCC structure belonging to the *Fm*3*m* space group. The characteristic peaks observed at 2θ = 11.4, 14.6, 16.3, 17.2, 18.9, 21.1, 23.9, 25.7, 29.2, 35.1, and 39.1° relate to (200), (220), (222), (400), (331), (422), (511), (500), (440), (660), (444), (731), (822), (733), and (882) planes and are in good agreement with the reported work.[53] In the XRD pattern of GO (given in inset), a peak at 11° with an interlayer distance corresponding to 8.8 Å was observed, which is typical of graphene oxide.[54] A well-defined similar pattern as reported earlier clearly indicates the presence of well-defined MOF units, and hence, GO did not act as a hindrance for the formation of Cu-MOF.

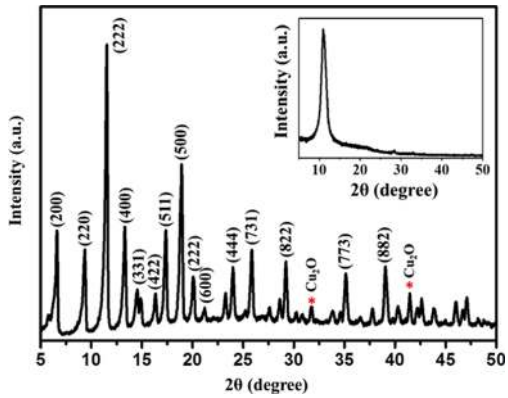

Figure 1. X-ray diffraction pattern of Cu-MOF/GO; the inset shows the XRD pattern of GO.

https://dx.doi.org/10.1021/acsomega.0c03170
ACS Omega 2020, 5, 23919−23930

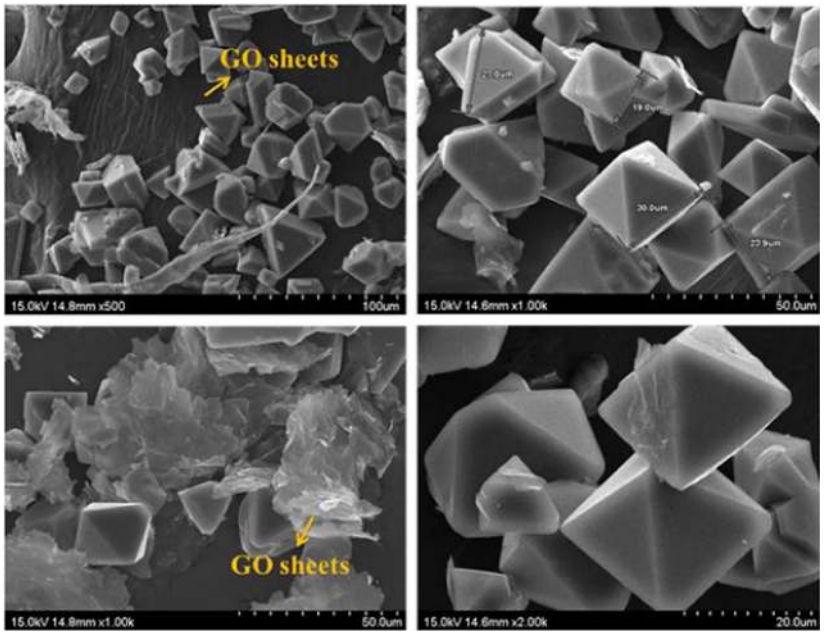

Figure 2. FE-SEM images of Cu-MOF/GO at various magnifications.

Consequently, the integration of GO did not disturb the crystal structure of MOF. Also, it could be observed from the pattern of the composite that the spectrum is dominated by the Cu-MOF structure with a GO peak at 11.4° overlapping with the MOF peak. The GO peak at 11° was not prominent, which could be because the content of GO was very less compared to that of the bulk MOF. Thus, the incorporation of GO did not disrupt the MOF crystal structure.

The textural structure of Cu-MOF/GO was analyzed by FE-SEM images (Figure 2). As can be seen from the images, the MOF possess cubic crystals with a truncated octahedral geometry and the crystalline sizes vary between 19 and 25 μm. Also, it could be observed that these Cu-MOF crystals are distributed on the graphene oxide sheets. Well-defined wrinkled graphene oxide layers with Cu-MOF crystals could be seen. The attractive forces and the interaction of MOF metal groups with the epoxy groups of graphene oxide are strong, thus leading to a synergistic effect. In an earlier report, it was stated that the MOF crystals are attached to the graphene layer due to the interaction between the metal sites of MOFs and the epoxy groups of GO.[43] Hence, the epoxy groups of GO prevented the aggregation of crystallites, leading to the well-defined structure. The average particle size of the synthesized Cu-BTC was calculated using Gaussian distribution, and the effect of particle size in addition to GO sheets was discussed. The average particle size was calculated to be 15.49 μm. In addition to GO, a few Cu-BTC particles are agglomerated to have 25 μm size. The distribution graph shows the particle variation from 5 to 25 μm as shown in Figure S1.

To further understand the thermal stability of the samples, thermogravimetric analysis (TGA) was performed, and the result is shown in Figure 3. The first weight loss of 12% below 20 °C is due to the dissolution of water molecules and solvents from the material. A smaller band around 200 °C is probably due to the removal of DMF molecules entrapped in the MOF cavities. The epoxy and carboxylic moieties get dissoluted away above 300 °C, in agreement with the literature.[41] This final weight loss above 300 °C could be attributed both to the

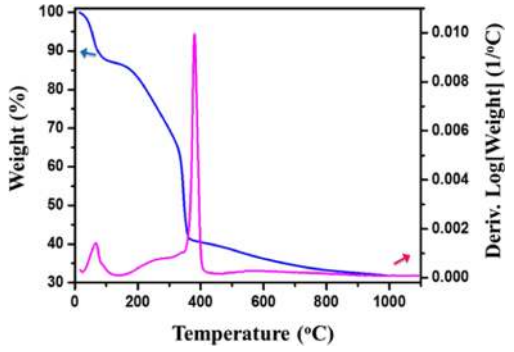

Figure 3. Thermogravimetric and differential calorimetric analyses of Cu-MOF/GO.

decomposition of MOFs and GO molecules. After decomposition, a ca. 32% of the remaining material remained in view of the remnant moieties, viz., oxides of Cu, Cu, and residual carbon. The specific heat of Cu-BTC was calculated to be 0.780 J/g K,[44] whereas the specific heat of the Cu-BTC/GO composite was 0.821 J/g K. This shows an increase of the activation energy to disintegrate the structure of CuBTC/GO, which confirms an increase in the stability of the prepared catalyst. The transition temperature of the prepared catalyst also increased from 340 to 380 °C.

To further explore the chemical nature of the material, XPS was used, and the spectra are shown in Figure 4, which reveals Cu, C, and O. C 1s could be deconvoluted to three peaks due to C−C of the aromatic system at 284.6 eV, C−O from epoxy, alkoxy observed at 286.2 eV, and finally O−C═O at 288.6 eV, and these peaks arise from the GO structure. In the case of Cu 2p, two Gaussian peaks could be seen at 934.6 due to the Cu $2p^{3/2}$ group and 954.5 eV due to Cu $2p^{1/2}$, respectively. Besides, shake-up satellite peaks between the two main peaks are characteristic of Cu(II) species. Similarly, O 1s peaks gave two deconvoluted peaks due to C−O and C═O groups, respectively.

https://dx.doi.org/10.1021/acsomega.0c03170
ACS Omega 2020, 5, 23919−23930

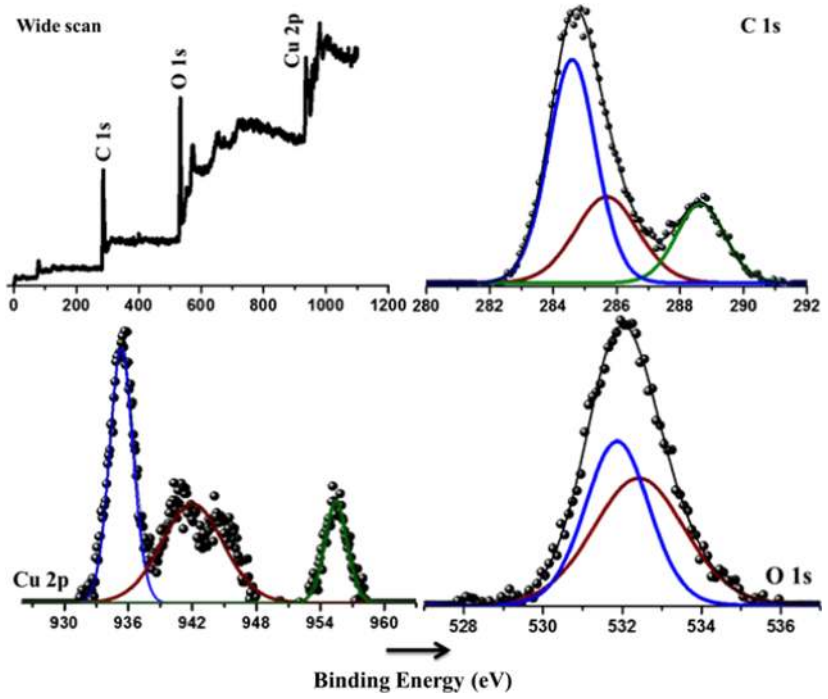

Figure 4. Wide-scan and deconvoluted XPS survey spectra of Cu-MOF/GO.

To access the porosity and surface area of the material, the Brunauer–Emmett–Teller (BET) analysis was used at 77 K under 1 atm, and the isotherm is shown in Figure 5. The surface area of the synthesized composite material was estimated to be 1332 m^2/g, which is slightly higher than those reported earlier for Cu-BTC alone, which means that the addition of GO to the MOF matrix has indeed increased its surface area. The porous capacity of the sample was measured using N_2 adsorption–desorption isotherms. The isotherms are nearly parallel over a wide relative pressure region of 0.5–1. This behavior suggests that the isotherms follow a typical type IV curve and an H4 type hysteresis loop. The first part of the type IV isotherm up to the relative pressure of 0.45 follows the same path ascribed to monolayer–multilayer adsorption. Similarly, the type H4 loop is related to slitlike pores.

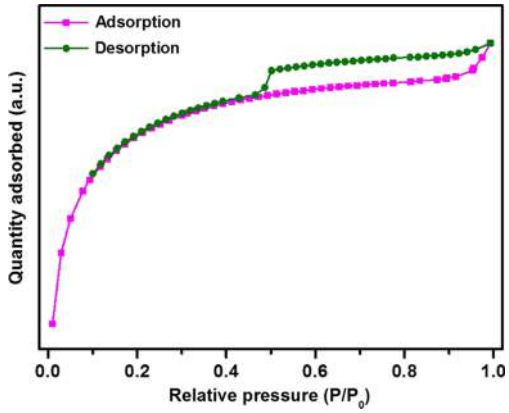

Figure 5. N_2 adsorption isotherms by the BET analysis of the Cu-MOF/GO composite.

Electrochemical Analysis of Cu-MOF/GO. The voltammetry technique is employed to explore the reduction of CO_2 and to determine its onset potential. In this regard, the current vs potential test was performed within the tested potential range. To test the electrocatalytic activity of the prepared catalyst, cyclic voltammetry of the prepared catalyst was performed in different electrolytes within the calculated potential regime at 50 mV/s in various supporting electrolytes,

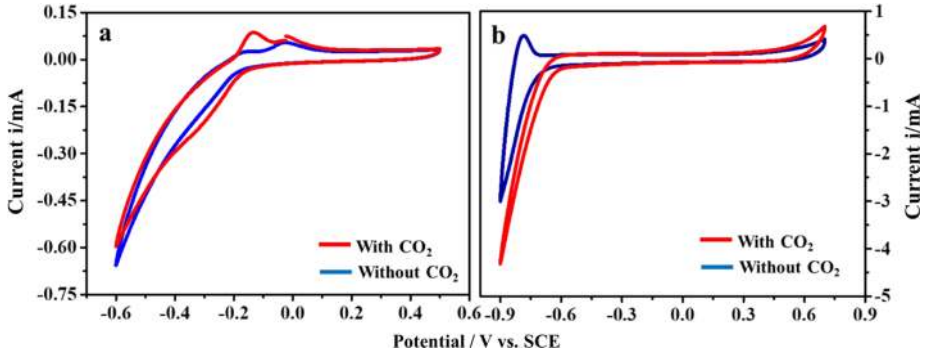

Figure 6. Current–potential curves of CO_2 reduction on the Cu-MOF/GO electrode in (a) 0.1 M $KHCO_3$ in water and (b) 0.1 M TBAB in DMF. Scan rate = 50 mV/s.

https://dx.doi.org/10.1021/acsomega.0c03170
ACS Omega 2020, 5, 23919–23930

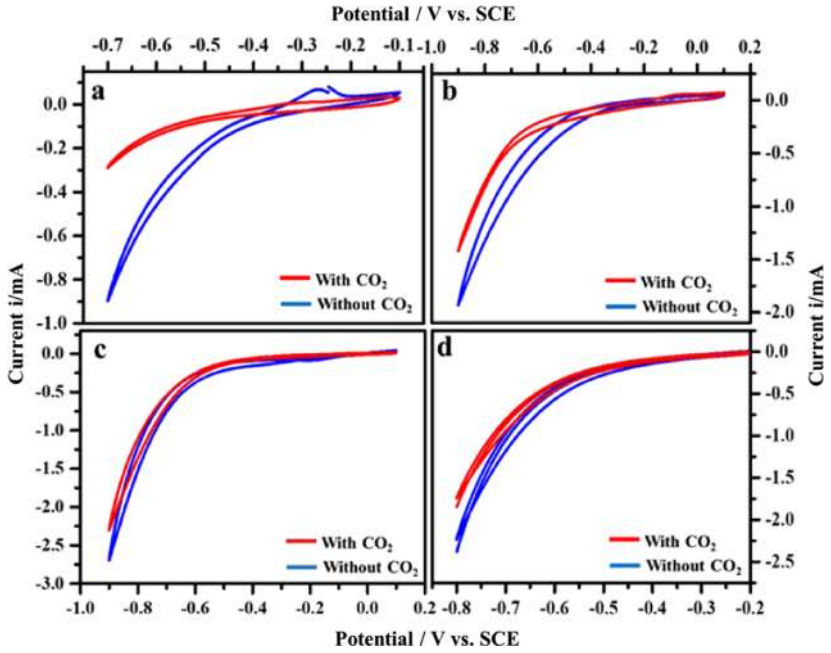

Figure 7. Current−potential curves of CO_2 reduction on the Cu-MOF/GO electrode in (a) 0.1 M KBr in methanol, (b) 0.1 M CH_3COOK in methanol, (c) 0.1 M TBAB in methanol, and (d) 0.1 M TBAP in methanol. Scan rate = 50 mV/s.

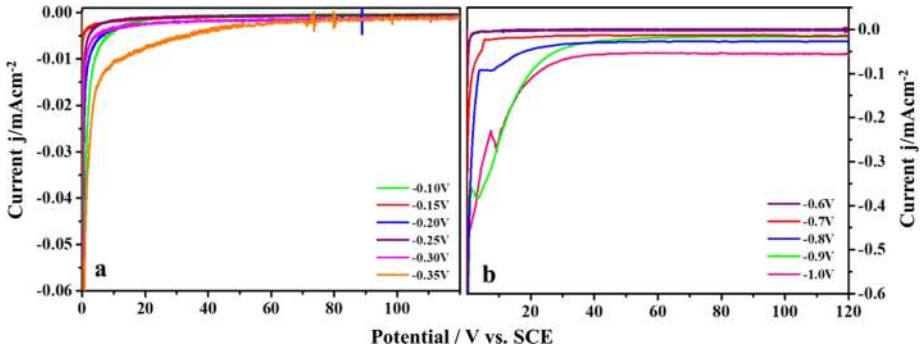

Figure 8. Current density profile obtained during CO_2 electroreduction at various potentiostatic electrolysis potentials for 120 min: (a) 0.1 M $KHCO_3$ in water and (b) 0.1 M TBAB in DMF.

viz., $KHCO_3/H_2O$, TBAB/DMF, KBr/CH_3OH, CH_3COOK/CH_3OH, $TBAB/CH_3OH$, and $TBAB/CH_3OH$, respectively. CO_2 was continuously bubbled into the cell to maintain a constant concentration throughout the experiment. Figures 6 and 7 demonstrate the $I-V$ graph of Cu-MOF/GO in the CO_2-saturated electrolyte. All of the CV's were run after optimizing the potential window where CO_2 reduction occurs. The cyclic voltammetric response reveals redox potential peaks in the negative scan corresponding to the Cu(0) to Cu(I) conversion. In the reduction side, a weak reduction peak is observed at the said potential. The onset potentials were acquired from the CV result. The onset potential values observed for all of the supporting electrolyte systems were approximately −0.1, −0.6, −0.4, −0.4, −0.3, and −0.4 V in $KHCO_3/H_2O$, TBAB/DMF, KBr/CH_3OH, CH_3COOK/CH_3OH, $TBAB/CH_3OH$, and $TBAP/CH_3OH$, respectively. In general, cyclic voltammetry measurements were performed to ascertain the onset potentials where CO_2 reduction begins. As observed from the tests, low onset potentials were observed for $KHCO_3/H_2O$ and $TBAB/CH_3OH$ as supporting electrolytes. In the case of 0.1 M $KHCO_3$, no voltammetric peaks were observed down to −0.6 V as further CO_2 reduction proceeded at an increasing negative potential. As observed in the cyclic voltammetric curves, from the onset potential value, the current density started increasing slowly till it reached −2.0 V after which a sharp increase in current was observed.

Constant-Potential Electrolysis. After the determination of the onset potentials from polarization experiments, further investigation was done to investigate the role of potential in product formation. The reduction process was carried out at a particular potential over a period of time. Constant-potential electrolysis of CO_2 in different electrolytes was performed at various potentials for a time period of 2 h (Figures 8 and 9). This will allow investigating the maximum amount of CO_2 reduction by the controlled potential electrolysis process. To perform this, the electrolyte was saturated with the analyte gas, viz., CO_2, for 1 h and throughout the electrolysis process. The electrolysis process was studied under similar experimental conditions like cyclic voltammetry. Electrolysis was carried out under a controlled atmosphere, and during the process, the output current and the product concentration due to reduction in the cell were examined as a function of time. Six different potentials closer to the onset potential were selected and applied as the input potential for the electrolysis process.

https://dx.doi.org/10.1021/acsomega.0c03170
ACS Omega 2020, 5, 23919−23930

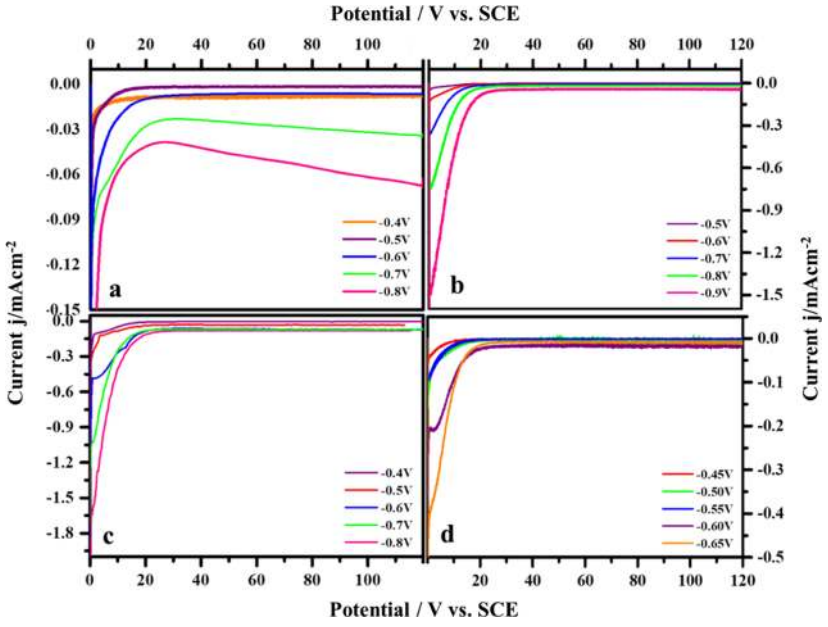

Figure 9. Current density profile obtained during CO_2 electroreduction at various potentiostatic electrolysis potentials for 120 min: (a) 0.1 M KBr in methanol, (b) 0.1 M CH_3COOK in methanol, (c) 0.1 M TBAB in methanol, and (d) 0.1 M TBAP in methanol.

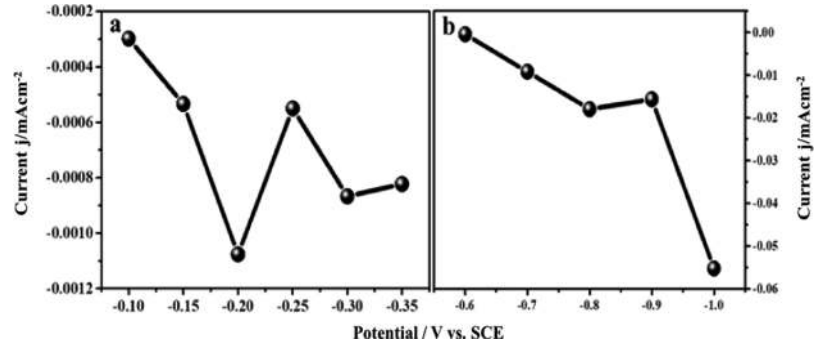

Figure 10. *I*–*V* plot of the CO_2 reduction: (a) 0.1 M $KHCO_3$ in water and (b) 0.1 M TBAB in DMF.

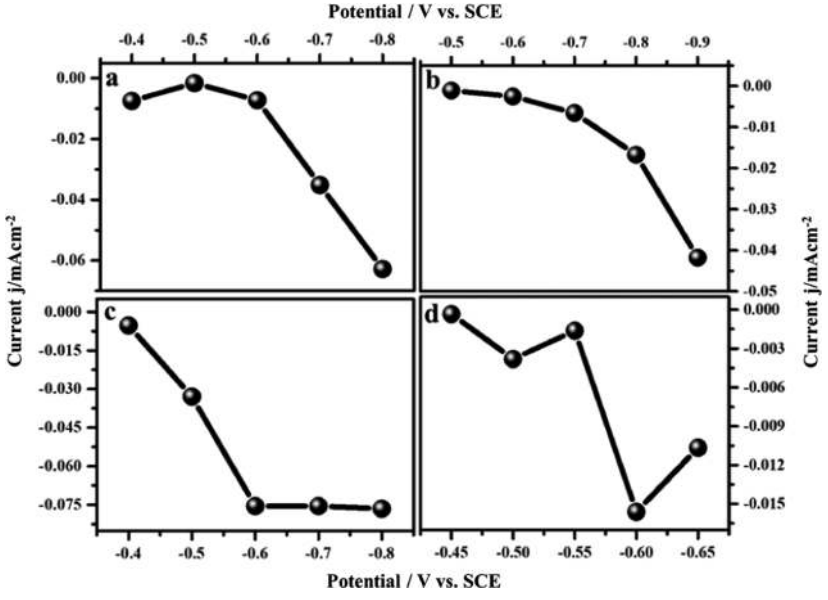

Figure 11. *I*–*V* plot of the CO_2 reduction: (a) 0.1 M KBr in methanol, (b) 0.1 M CH_3COOK in methanol, (c) 0.1 M TBAB in methanol, and (d) 0.1 M TBAP in methanol.

https://dx.doi.org/10.1021/acsomega.0c03170
ACS Omega 2020, 5, 23919−23930

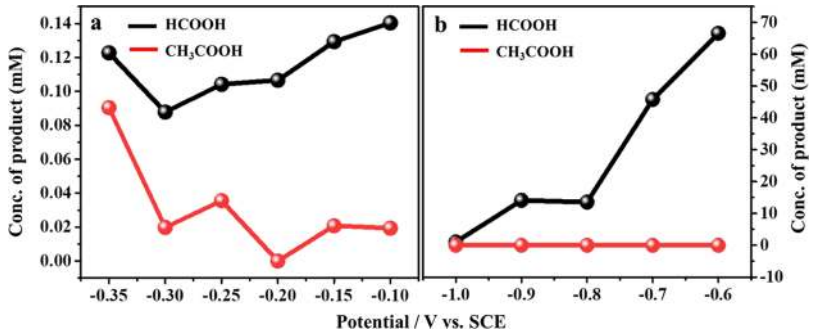

Figure 12. Concentration of the product at various potentials applied: (a) 0.1 M $KHCO_3$ in water and (b) 0.1 M TBAB in DMF.

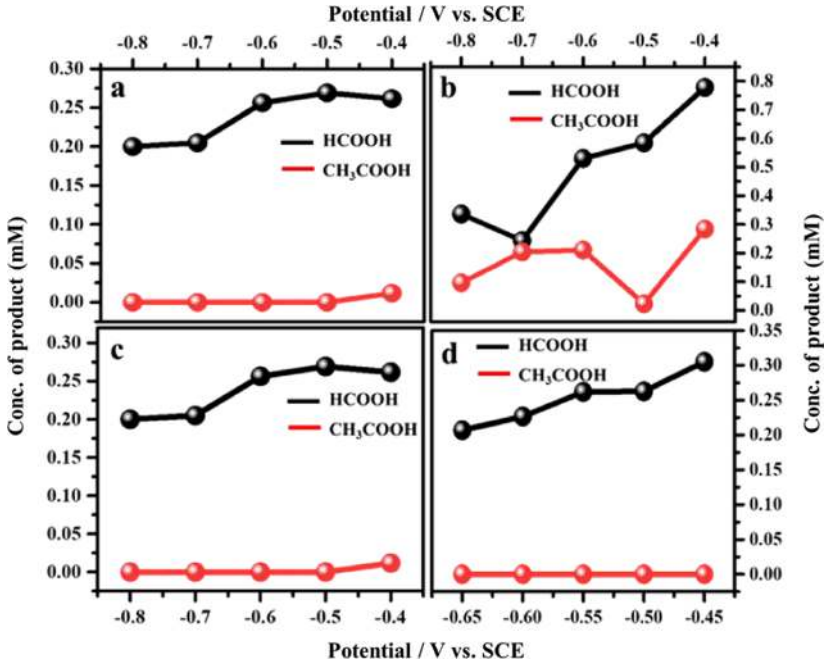

Figure 13. Concentration of the product at various potentials applied: (a) 0.1 M KBr in methanol, (b) 0.1 M CH_3COOK in methanol, (c) 0.1 M TBAB in methanol and (d) 0.1 M TBAP in methanol.

CO_2 reduction was tested in all of the supporting electrolytes at various potentials. For all of the cases, the efficiency of product formation was investigated by analyzing the concentration of the formed product by ion chromatography and the corresponding stationary $I-V$ plot extracted from CA analysis, as shown in Figures 10 and 11. From the figure, it can be observed that at higher potentials, the efficiency in terms of current becomes less, owing to the less reduction process happening, which indicates that the whole process of transport of CO_2 gas is via diffusion. After the process, the sample was withdrawn to know the nature of the formed product.

As observed in the figure, the major product was formic acid with a minor formation of acetic acid. In the $KHCO_3$ electrolyte, the current densities are more limited at a potential less than −0.25 V and a regular trend was not observed. Almost in all of the electrolytes, the current density declined linearly with an increase in negative potentials. In the case of TBAP as the electrolyte, a maximum current density was seen at a potential of −0.55 V (Figure 11d). For the 0.1 M $KHCO_3/H_2O$ system, the rate of formation of the products increased from −0.35 V and reached a maximum at −0.1 V. Thus, for this electrolyte, the HCOOH formation rate was high at −0.1 V, and thus, this potential was fixed for the CO_2 reduction process. A series of tests were done to investigate the effect of supporting electrolyte on product formation. Before probing the role of the supporting electrolyte, the system was checked in DMF and methanol systems with $KHCO_3$ and TBAB as supporting electrolytes.

In both the cases, HCOOH and CH_3COOH were obtained but their concentrations were very low. Although the mechanism was unclear, the system was reinvestigated to increase the product yield with an emphasis focused on formic acid. In this view, different supporting electrolytes were tested, viz., KBr, CH_3COOK, TBAB, and TBAP, with methanol as the electrolyte. Methanol was chosen in view of its high solubility factor for the CO_2 analyte, which is 5 times more than water.[55] Later, the sample was withdrawn to know about the nature of the product. As seen from the graphs, TBAB in DMF gave a higher concentration of formic acid, viz., 66.57 mM, but there was no trace of the formation of acetic acid. This was the same with other supporting electrolyte, viz., CH_3COOK and TBAP, which gave only formic acid as the main product. To further know the effect of applied potential on product formation, a range of potentials were applied for CO_2 electroreduction. To compare, electroreduction was carried out with Cu-MOF alone

https://dx.doi.org/10.1021/acsomega.0c03170
ACS Omega 2020, 5, 23919−23930

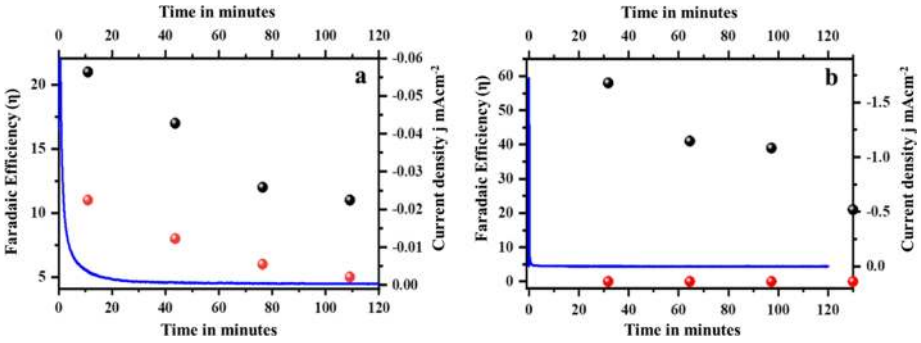

Figure 14. Current density profiles and faradic efficiencies of CO_2 reduction: (a) CH_3COOH in methanol at −0.5 V and (b) KBr in methanol at −0.5 V.

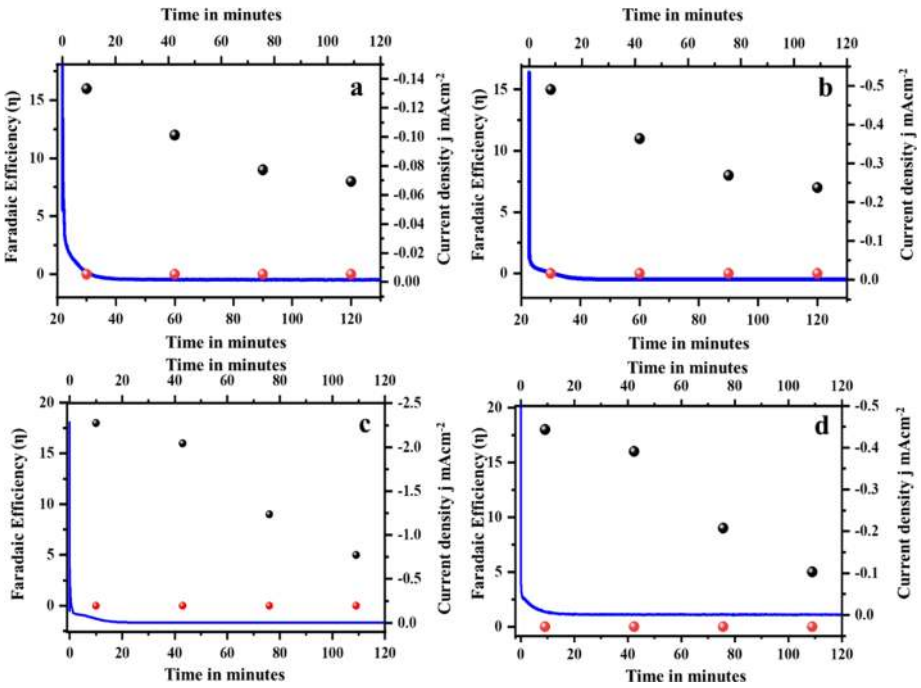

Figure 15. Current density profiles and faradic efficiencies of CO_2 reduction: (a) $KHCO_3$ in water at −0.1 V, (b) TBAB in methanol at −0.4 V, (c) TBAP in methanol at −0.5 V, and (d) TBAB in DMF at 0.6 V.

without GO and is shown in Figures S2 and S3. Figure S2a shows the CV curve of CO_2 reduction and the reduction process is carried out at different potentials (Figure S2b) over a period of 2 h. Further, from the *I*−*V* plot, it could be seen that the reduction was more at −0.6 V vs SCE (Figure S3a) and HCOOH was the main product (Figure S3). At −0.6 V, the maximum concentration of HCOOH was observed to be 40.12 mM.

The applied potentials were optimized by running a voltammetric experiment before electrolysis. For TBAP, the concentration of HCOOH increases with the applied potential followed by a decline after −0.65 V (Figures 12 and 13). At −0.8 V vs SCE, the rate of formation of HCOOH reached a maximum. The highest concentrations of formic acid formed for different electrolytes are 0.1404 mM (−0.1 V), 66.57 mM (−0.6 V), 0.2651 mM (−0.5 V), 0.2359 mM (−0.5 V), 0.7784 mM (−0.4 V), and 0.3050 mM (−0.45 V) in various electrolytes, viz., $KHCO_3/H_2O$, TBAB/DMF, KBr/CH_3OH, CH_3COOK/CH_3OH, $TBAB/CH_3OH$, and $TBAP/CH_3OH$, respectively.

The faradic efficiency was calculated to be 21, 58, 16, 15, 28, and 18%, respectively, for formic acid for the different electrolytes (Figures 14 and 15). In the case of Cu-MOF alone, the faradic efficiency was calculated to be 38%. In general, Cu-based systems are more suitable for CO_2 adsorption.[56] It is well known that CO_2 is an acidic molecule and hence will get attracted easily with electron donors like Cu^{2+} in Cu-MOF, which might be the reason for effective CO_2 reduction to formic acid. Hence, the basicity of Cu in MOF structures attracts the gas molecules adhering to the electrodes, thereby facilitating the reduction process, and graphene oxide aids the process owing to its excellent conductivity. GO has several advantages with regard to efficiency, not only owing to its unique electrical and physical properties but also rGO being a support material for the MOF network, thus providing a synergistic effect. Although the efficiency is good, more work has to be done to comprehend the exact effect of the catalyst material and the supporting electrolyte. This type of work will lead to the production of liquid fuels from low-priced catalyst materials. The rate of the reaction is shown in Figure S4. The faradic efficiency of CO_2 reduction in the TBAB/DMF

https://dx.doi.org/10.1021/acsomega.0c03170
ACS Omega 2020, 5, 23919−23930

electrolyte was calculated to be 58% with a reaction rate of 800 nmol/hcm^2. A table of comparison of the formation rates of formic acid using various catalysts reported is given in Table S1. In this, high formate production of the catalyst due to the formic acid pathway occurs due to high charge-transfer rate, whereas low formate production is due to the carbonyl pathway.[67]

CONCLUSIONS

This work reported the CO_2 reduction process via an electrochemical route through electrolysis at a constant potential, and for finding the role of the electrolytes, the reaction was carried out in six different supporting electrolytes, viz., $KHCO_3/H_2O$, TBAB/DMF, KBr/CH_3OH, CH_3COOK/CH_3OH, TBAB/CH_3OH, and TBAP/CH_3OH. As observed from the tests, a less onset potential was observed for $KHCO_3$/H_2O and TBAB/CH_3OH supporting electrolytes. The results revealed the formation of HCOOH as the main product in all of the electrolytes. The highest concentrations of formic acid formed for different electrolytes are 0.1404 mM (−0.1 V), 66.57 mM (−0.6 V), 0.2651 mM (−0.5 V), 0.2359 mM (−0.5 V), 0.7784 mM (−0.4 V), and 0.3050 mM (−0.45 V) in various electrolytes, viz., $KHCO_3/H_2O$, TBAB/DMF, KBr/CH_3OH, CH_3COOK/CH_3OH, TBAB/CH_3OH, and TBAP/CH_3OH, respectively. The results revealed a high efficiency of 58% obtained with 0.1 M TBAB/DMF electrolyte. Thus, the overall results demonstrated that the reported process showed the formation of HCOOH and CH_3COOH products with the synthesized MOF material.

ASSOCIATED CONTENT

Supporting Information

The Supporting Information is available free of charge at https://pubs.acs.org/doi/10.1021/acsomega.0c03170.

Particle size distribution curve for the Cu-BTC/GO composite (Figure S1), current−potential curves of CO_2 reduction and current density profile on the Cu-MOF electrode (Figure S2), I−V plot of CO_2 reduction and concentration of the product at various potentials applied (Figure S3), conversion rates vs applied potential (Figure S4), and comparison on the rate of the formation of formic acid with the literature (Table S1) (PDF)

AUTHOR INFORMATION

Corresponding Authors

Andrews Nirmala Grace − *Centre for Nanotechnology Research, Vellore Institute of Technology, Vellore 632014, India;* orcid.org/0000-0002-2016-3013; Email: anirmalaglady s@gmail.com

Soon Kwan Jeong − *Climate Change Technology Research Division, Korea Institute of Energy Research, Daejeon 305-343, Korea;* orcid.org/0000-0001-5347-3651; Email: jeongsk@kier.re.kr

Authors

Sun-Mi Hwang − *Climate Change Technology Research Division, Korea Institute of Energy Research, Daejeon 305-343, Korea*

Song Yi Choi − *Catalytic Materials Research Department, KORENS RTX, Gyeryong-si, Chungcheongnam-do 328-42, Korea*

Min Hye Youn − *Climate Change Technology Research Division, Korea Institute of Energy Research, Daejeon 305-343, Korea*

Wonhee Lee − *Climate Change Technology Research Division, Korea Institute of Energy Research, Daejeon 305-343, Korea*

Ki Tae Park − *Climate Change Technology Research Division, Korea Institute of Energy Research, Daejeon 305-343, Korea*

Kannan Gothandapani − *Centre for Nanotechnology Research, Vellore Institute of Technology, Vellore 632014, India*

Complete contact information is available at: https://pubs.acs.org/10.1021/acsomega.0c03170

Notes

The authors declare no competing financial interest.

ACKNOWLEDGMENTS

This work was supported by the Energy Demand Side Management Program of the Korea Institute of Energy Technology Evaluation and Planning (KETEP) funded by the Ministry of Trade, Industry & Energy, Republic of Korea (No. 20182010202100).

REFERENCES

(1) Figueroa, J. D.; Timothy, F.; Sean, P.; Howard, M.; Rameshwar, D. S. Advances in CO_2 capture technology-the US Department of Energy's Carbon Sequestration Program. *Int. J. Greenhouse Gas Control* **2008**, *2*, 9−20.

(2) Lv, W.; Jingjing, B.; Rui, Z.; Wenjuan, W.; Fenying, K.; Lei, W.; Wang, W. $Bi_2O_2CO_3$ nanosheets as electrocatalysts for selective reduction of CO_2 to formate at low overpotential. *ACS Omega* **2017**, *2*, 2561−2567.

(3) Olajire, A. CO_2 capture and separation technologies for end-of-pipe applications−a review. *Energy* **2010**, *35*, 2610−2628.

(4) MacDowell, N.; Nick, F.; Antoine, B.; Jason, H.; Amparo, G.; George, J.; Adjiman, C. S.; Williams, C. K.; Nilay, S.; Paul, F. An overview of CO_2 capture technologies. *Energy Environ. Sci.* **2010**, *3*, 1645−1669.

(5) Park, S.-M.; Razzaq, A.; Park, Y. H.; Saurav, S.; Yiseul, P.; Grimes, C. A.; Su-Il, I. Hybrid Cu_xO−TiO_2 Heterostructured Composites for Photocatalytic CO_2 Reduction into Methane Using Solar Irradiation: Sunlight into Fuel. *ACS Omega* **2016**, *1*, 868−875.

(6) *Electrochemical and Electrocatalytic Reactions of Carbon Dioxide*; 1st ed.; In Sullivan, B.; Patrick, K. K.; Guard, H. E., Eds.; Elsevier, 2012; pp 1−268.

(7) Olah, G. A.; Alain, G.; Prakash, G. K. S. Chemical recycling of carbon dioxide to methanol and dimethyl ether: from greenhouse gas to renewable, environmentally carbon neutral fuels and synthetic hydrocarbons. *J. Org. Chem.* **2009**, *74*, 487−498.

(8) Olah, G. A.; Prakash, G. K. S.; Goeppert, A. Anthropogenic chemical carbon cycle for a sustainable future. *J. Am. Chem. Soc.* **2011**, *133*, 12881−12898.

(9) Gattrell, M.; Gupta, N.; Co, A. A review of the aqueous electrochemical reduction of CO_2 to hydrocarbons at copper. *J. Electroanal. Chem.* **2006**, *594*, 1−19.

(10) Wang, Y.; Cailing, N.; Dunwei, W. Metallic nanocatalysts for electrochemical CO_2 reduction in aqueous solutions. *J. Colloid Interface Sci.* **2018**, *527*, 95−106.

(11) Zhu, W.; Ronald, M.; Önder, M.; Haifeng, L. V.; Shaojun, G.; Christopher, J. W.; Xiaolian, S.; Andrew, A. P.; Shouheng, S. Monodisperse Au nanoparticles for selective electrocatalytic reduction of CO_2 to CO. *J. Am. Chem. Soc.* **2013**, *135*, 16833−16836.

(12) Benson, E. E.; Clifford, P. K.; Aaron, J. S.; Jonathan, M. S. Electrocatalytic and homogeneous approaches to conversion of CO_2 to liquid fuels. *Chem. Soc. Rev.* **2009**, *38*, 89−99.

(13) Bard, A. J. Inner-sphere heterogeneous electrode reactions. Electrocatalysis and photocatalysis: the challenge. *J. Am. Chem. Soc.* **2010**, *132*, 7559−7567.
(14) Hori, Y. I. Electrochemical CO_2 Reduction on Metal Electrodes. In *Modern Aspects of Electrochemistry*; Springer: New York, 2008; pp 89−189.
(15) Ohta, K.; Kawamoto, M.; Mizuno, T.; Lowy, D. A. Electrochemical reduction of carbon dioxide in methanol at ambient temperature and pressure. *J. Appl. Electrochem.* **1998**, *28*, 717−724.
(16) Chen, Y.; Christina, W. L.; Matthew, W. K. Aqueous CO_2 reduction at very low overpotential on oxide-derived Au nanoparticles. *J. Am. Chem. Soc.* **2012**, *134*, 19969−19972.
(17) Khezri, B.; Adrian, C. F.; Martin, P. CO_2 reduction: the quest for electrocatalytic materials. *J. Mater. Chem. A* **2017**, *5*, 8230−8246.
(18) Kaneco, S.; Kenji, I.; Kiyohisa, O.; Takayuki, M.; Akira, S. Electrochemical reduction of CO_2 on Au in KOH^+ methanol at low temperature. *J. Electroanal. Chem.* **1998**, *441*, 215−220.
(19) Kaneco, S.; Kenji, I.; Nobu-Hide, H.; Kiyohisa, O.; Takayuki, M.; Tohru, S. Electrochemical reduction of carbon dioxide to ethylene with high Faradaic efficiency at a Cu electrode in CsOH/methanol. *Electrochim. Acta* **1999**, *44*, 4701−4706.
(20) Ogura, K.; Hiroshi, Y.; Takayasu, T. Selective formation of ethylene from CO_2 by catalytic electrolysis at a three-phase interface. *Catal. Today* **2004**, *98*, 515−521.
(21) Dubé, P.; Brisard, G. M. Influence of adsorption processes on the CO2 electroreduction: An electrochemical mass spectrometry study. *J. Electroanal. Chem.* **2005**, *582*, 230−240.
(22) Kaneco, S.; Hideyuki, K.; Tohru, S.; Kiyohisa, O. Electrochemical reduction of carbon dioxide to ethylene at a copper electrode in methanol using potassium hydroxide and rubidium hydroxide supporting electrolytes. *Electrochim. Acta* **2006**, *51*, 3316−3321.
(23) Gupta, N.; Gattrell, M.; Dougall, B. M. Calculation for the cathode surface concentrations in the electrochemical reduction of CO_2 in $KHCO_3$ solutions. *J. Appl. Electrochem.* **2006**, *36*, 161−172.
(24) Taguchi, S.; Akiko, A. Surface-structure sensitive reduced CO_2 formation on Pt single crystal electrodes in sulfuric acid solution. *Electrochim. Acta* **1994**, *39*, 2533−2537.
(25) Hori, Y.; Konishi, H.; Futamura, T.; Murata, A.; Koga, O.; Sakurai, H.; Oguma, K. Deactivation of copper electrode" in electrochemical reduction of CO_2. *Electrochim. Acta* **2005**, *50*, 5354−5369.
(26) Hernández, R. M.; Márquez, Jairo.; Márquez, O. P.; Choy, M.; Ovalles, C.; Garcia, J. J.; Scharifker, B. Reduction of carbon dioxide on modified glassy carbon electrodes. *J. Electrochem. Soc.* **1999**, *146*, 4131−4136.
(27) Jitaru, M. Electrochemical carbon dioxide reduction-fundamental and applied topics. *J. Univ. Chem. Technol. Metall.* **2007**, *4*, 333−344.
(28) Sun, Z.; Tao, M.; Hengcong, T.; Qun, F.; Buxing, H. Fundamentals and challenges of electrochemical CO_2 reduction using two-dimensional materials. *Chem* **2017**, *3*, 560−587.
(29) Köleli, F.; Atilan, T.; Palamut, N.; Gizir, A. M.; Aydin, R.; Hamann, C. H. Electrochemical reduction of CO_2 at Pb-and Sn-electrodes in a fixed-bed reactor in aqueous K_2CO_3 and $KHCO_3$ media. *J. Appl. Electrochem.* **2003**, *33*, 447−450.
(30) Kim, H.; Hyunju, L.; Taeho, L.; Sang, H. A. Facile fabrication of porous Sn-based catalysts for electrochemical CO_2 reduction to HCOOH and syngas. *J. Ind. Eng. Chem.* **2018**, *66*, 248−253.
(31) Kaneco, S.; Hideyuki, K.; Tohru, S.; Kiyohisa, O. Electrochemical reduction of CO_2 to methane at the Cu electrode in methanol with sodium supporting salts and its comparison with other alkaline salts. *Energy Fuels* **2006**, *20*, 409−414.
(32) Wu, Y.; Xianghai, S.; Shuai, L.; Jiahui, Z.; Xinghui, Y.; Pengxin, S.; Lijing, G.; Ruiping, W.; Jin, Z.; Guomin, X. 3D-monoclinic M−BTC MOF (M = Mn, Co, Ni) as highly efficient catalysts for chemical fixation of CO_2 into cyclic carbonates. *J. Ind. Eng. Chem.* **2018**, *58*, 296−303.
(33) Aydin, R.; Köleli, F. Electrocatalytic conversion of CO_2 on a polypyrrole electrode under high pressure in methanol. *Synth. Met.* **2004**, *144*, 75−80.
(34) Ogura, K.; Hiroshi, Y.; Fukutaro, S. Catalytic reduction of CO_2 to ethylene by electrolysis at a three-phase interface. *J. Electrochem. Soc.* **2003**, *150*, D163−D168.
(35) Yano, H.; Tanaka, T.; Nakayama, M.; Ogura, K. Selective electrochemical reduction of CO_2 to ethylene at a three-phase interface on copper (I) halide-confined Cu-mesh electrodes in acidic solutions of potassium halides. *J. Electroanal. Chem.* **2004**, *565*, 287−293.
(36) Ogura, K.; Oohara, R.; Kudo, Y. Reduction of CO_2 to ethylene at three-phase interface effects of electrode substrate and catalytic coating. *J. Electrochem. Soc.* **2005**, *152*, D213−D219.
(37) Kulandaivalu, T.; Rashid, S. A.; Sabli, T.; Ling, T. Visible light assisted photocatalytic reduction of CO_2 to ethane using CQDs/Cu_2O nanocomposite photocatalyst. *Diamond Relat. Mater.* **2019**, *91*, 64−73.
(38) Vasileff, A.; Xing, Z.; Chaochen, X.; Lei, G.; Yan, J.; Yao, Z.; Shi-Zhang, Q. Selectivity control for electrochemical CO_2 reduction by charge redistribution on the surface of copper alloys. *ACS Catal.* **2019**, *9*, 9411−9417.
(39) Mao, J.; Lifen, Y.; Ping, Y.; Xianwen, W.; Lanqun, M. Electrocatalytic four-electron reduction of oxygen with Copper (II)-based metal-organic frameworks. *Electrochem. Commun.* **2012**, *19*, 29−31.
(40) Senthil Kumar, R.; Senthil Kumar, S.; Kulandainathan, M. A. Highly selective electrochemical reduction of carbon dioxide using Cu based metal organic framework as an electrocatalyst. *Electrochem. Commun.* **2012**, *25*, 70−73.
(41) Zhang, Y.; Xiangjie, B.; Charles, L.; Huan, W.; Mian, L.; Liping, G. Facile synthesis of a Cu-based MOF confined in macroporous carbon hybrid material with enhanced electrocatalytic ability. *Chem. Commun.* **2013**, *49*, 6885−6887.
(42) Nivetha, R.; Pratap, K.; Krishna, C.; Sudhagar, P.; Soon, K. J.; Andrews, N. G. Role of MIL-53 (Fe)/hydrated−dehydrated MOF catalyst for electrochemical hydrogen evolution reaction (HER) in alkaline medium and photocatalysis. *RSC Adv.* **2019**, *9*, 3215−3223.
(43) Petit, C.; Teresa, J. B. MOF−graphite oxide composites: combining the uniqueness of graphene layers and metal−organic frameworks. *Adv. Mater.* **2009**, *21*, 4753−4757.
(44) Qian, D.; Cheng, L.; Guang-Ping, H.; Li, W.-C.; Lu, A.-H. Synthesis of hierarchical porous carbon monoliths with incorporated metal−organic frameworks for enhancing volumetric based CO_2 capture capability. *ACS Appl. Mater. Interfaces* **2012**, *4*, 6125−6132.
(45) Pachfule, P.; Beena, K. B.; Sreekumar, K.; Rahul, B. One-dimensional confinement of a nanosized metal organic framework in carbon nanofibers for improved gas adsorption. *Chem. Commun.* **2012**, *48*, 2009−2011.
(46) Li, Q.; Wenlei, Z.; Jiaju, F.; Hongyi, Z.; Gang, W.; Shouheng, S. Controlled assembly of Cu nanoparticles on pyridinic-N rich graphene for electrochemical reduction of CO_2 to ethylene. *Nano Energy* **2016**, *24*, 1−9.
(47) Zhang, Z.; Fawad, A.; Wanghui, Z.; Wensheng, Y.; Wenhua, Z.; Hongwen, H.; Chao, M.; Jie, Z. Enhanced electrocatalytic reduction of CO_2 via chemical coupling between indium oxide and reduced graphene oxide. *Nano Lett.* **2019**, *19*, 4029−4034.
(48) Lim, D.-H.; Jun, H. J.; Dong, Y. S.; Jennifer, W.; Hyung, C. H.; Suk, W. N. Carbon dioxide conversion into hydrocarbon fuels on defective graphene-supported Cu nanoparticles from first principles. *Nanoscale* **2014**, *6*, 5087−5092.
(49) Geioushy, R. A.; Mazen, M. K.; Abbas, S. H.; Khalid, A.; Chanbasha, B. High efficiency graphene/Cu_2O electrode for the electrochemical reduction of carbon dioxide to ethanol. *J. Electroanal. Chem.* **2017**, *785*, 138−143.
(50) Hossain, M. N.; Zhonggang, L.; Jiali, W.; Aicheng, C. Enhanced catalytic activity of nanoporous Au for the efficient electrochemical reduction of carbon dioxide. *Appl. Catal., B* **2018**, *236*, 483−489.

https://dx.doi.org/10.1021/acsomega.0c03170
ACS Omega 2020, 5, 23919−23930

(51) Grace, A. N.; Song, Y.; Mari, V.; Margandan, B.; Dae, H. C.; Yeoil, Y.; Sung, C. N.; Soon, K. J. Electrochemical reduction of carbon dioxide at low overpotential on a polyaniline/Cu_2O nanocomposite based electrode. *Appl. Energy* **2014**, *120*, 85−94.
(52) Yaqoob, L.; Tayyaba, N.; Naseem, I.; Habib, N.; Manzar, S.; Neelam, Z.; Muhammad, U. Nanocomposites of cobalt benzene tricarboxylic acid MOF with rGO: An efficient and robust electocatalyst for oxygen evaluation reaction (OER). *Renewable Energy* **2020**, *156*, 1040−1054.
(53) Rizvi, S. A. M.; Naseem, I.; Muhammad, D. H.; Tayyaba, N.; Rehan, A.; Saadia, H. Synthesis and Characterization of Cu-MOF Derived Cu@ AC Electrocatalyst for Oxygen Reduction Reaction in PEMFC. *Catal. Lett.* **2020**, *150*, 1397−1407.
(54) Haider, M. D.; Naseem, I.; Syed, A. M. R.; Tayyaba, N.; Saadia, H.; Rehan, A. ZIF-67 derived Cu doped electrocatalyst for oxygen reduction reaction. *J. Electrochem. Energy Convers. Storage* **2020**, *18*, No. 021001.
(55) Noor, T.; Muhammad, A.; Neelam, Z.; Naseem, I.; Lubna, Y.; Habib, N. A highly efficient and stable copper BTC metal organic framework derived electrocatalyst for oxidation of methanol in DMFC application. *Catal. Lett.* **2019**, *149*, 3312−3327.
(56) Albo, J.; Alfonso, S.; Jose, S.-G.; Vicente, M.; Irabien, A. Production of methanol from CO_2 electroreduction at Cu_2O and Cu_2O/ZnO-based electrodes in aqueous solution. *Appl. Catal., B* **2015**, *176−177*, 709−717.
(57) Albo, J.; Angel, I. Cu_2O-loaded gas diffusion electrodes for the continuous electrochemical reduction of CO_2 to methanol. *J. Catal.* **2016**, *343*, 232−239.
(58) Albo, J.; Garikoitz, B.; Castaño, P.; Irabien, A. Methanol electrosynthesis from CO_2 at Cu_2O/ZnO prompted by pyridine-based aqueous solutions. *J. CO_2 Util.* **2017**, *18*, 164−172.
(59) Albo, J.; Daniel, V.; Garikoitz, B.; Castillo, O.; Castaño, P.; Irabien, A. Copper-based metal−Organic porous materials for CO_2 electrocatalytic reduction to alcohols. *ChemSusChem* **2017**, *10*, 1100−1109.
(60) Albo, J.; Maite, P.-I.; Garikoitz, B.; Angel, I. Cu/Bi metal-organic framework-based systems for an enhanced electrochemical transformation of CO_2 to alcohols. *J. CO_2 Util.* **2019**, *33*, 157−165.
(61) Santos-Lorenzo, J.; Rubén, S. J.-V.; Jonathan, A.; Garikoitz, B.; Pedro, C.; Oscar, C.; Antonio, L.; Sonia, P.-Y. A straightforward route to obtain zirconium based metal-organic gels. *Microporous Mesoporous Mater.* **2019**, *284*, 128−132.
(62) Chui, S. S.-Y.; Samuel, M.-F. L.; Charmant, J. P. H.; Orpen, A. G.; Ian, D. W. A chemically functionalizable nanoporous material $[Cu_3(TMA)_2(H_2O)_3]$n. *Science* **1999**, *283*, 1148−1150.
(63) Dhakshinamoorthy, A.; Mercedes, A.; Hermenegildo, G. Aerobic oxidation of benzylic alcohols catalyzed by metal− organic frameworks assisted by TEMPO. *ACS Catal.* **2011**, *1*, 48−53.
(64) Ramachandran, R.; Sathiyanathan, F.; Girish, M. J.; Raghupathy, B. P. C.; Soon, K. J.; Andrews, N. G. Synthesis of graphene platelets by chemical and electrochemical route. *Mater. Res. Bull.* **2013**, *48*, 3834−3842.
(65) Kaneco, S.; Hiei, N.-H.; Xing, Y.; Katsumata, H.; Ohnishi, H.; Suzuki, T.; Ohta, K. Electrochemical conversion of carbon dioxide to methane in aqueous $NaHCO_3$ solution at less than 273 K. *Electrochim. Acta* **2002**, *48*, 51−55.
(66) Kim, B. J.; Cho, K.-S.; Park, S.-J. Copper oxide-decorated porous carbons for carbon dioxide adsorption behaviors. *J. Colloid Interface Sci.* **2010**, *342*, 575−578.
(67) Fu, Y.; Yanan, L.; Xia, Z.; Yuyu, L.; Xiaodong, Z.; Jinli, Q. Electrochemical CO_2 reduction to formic acid on crystalline SnO_2 nanosphere catalyst with high selectivity and stability. *Chin. J. Catal.* **2016**, *37*, 1081−1088.

https://dx.doi.org/10.1021/acsomega.0c03170
ACS Omega 2020, 5, 23919−23930